RSC Advances

This is an *Accepted Manuscript*, which has been through the Royal Society of Chemistry peer review process and has been accepted for publication.

Accepted Manuscripts are published online shortly after acceptance, before technical editing, formatting and proof reading. Using this free service, authors can make their results available to the community, in citable form, before we publish the edited article. This *Accepted Manuscript* will be replaced by the edited, formatted and paginated article as soon as this is available.

You can find more information about *Accepted Manuscripts* in the Information for Authors.

Please note that technical editing may introduce minor changes to the text and/or graphics, which may alter content. The journal's standard Terms & Conditions and the Ethical guidelines still apply. In no event shall the Royal Society of Chemistry be held responsible for any errors or omissions in this *Accepted Manuscript* or any consequences arising from the use of any information it contains.

ROYAL SOCIETY OF CHEMISTRY

www.rsc.org/advances

Graphical Abstract

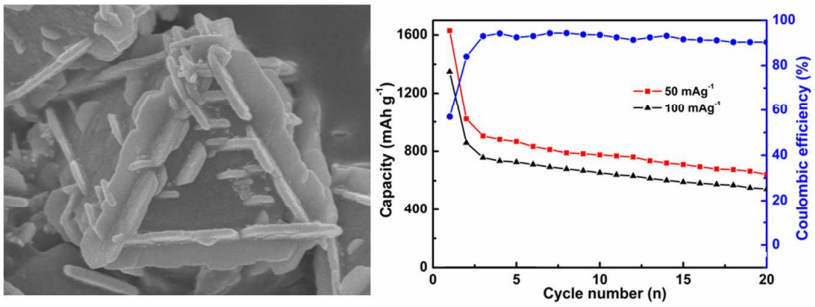

RSC Advances Accepted Manuscript

Cite this: DOI: 10.1039/c0xx00000x

www.rsc.org/xxxxxx

ARTICLE TYPE

Surfactant-free synthesis of Zn_2SnO_4 octahedron decorated with nanoplates and its application in rechargeable lithium ion batteries

Hongmin Fan, [a,b] Zhifang Liu, [a,b] Jiaqin Yang, [a,b] Caiying Wei, [a,b] Jing Zhang, [a,b] Liyan Wu, [a,b] Wenjun Zheng* [a,b]

Received (in XXX, XXX) Xth XXXXXXXXX 200X, Accepted Xth XXXXXXXXX 200X
DOI: 10.1039/b000000x

We demonstrate the fabrication of Zn_2SnO_4 octahedron decorated with nanoplates via a facile surfactant-free hydrothermal method. A high initial discharge capacity of 1629.9 mAh g^{-1} is obtained and the capacity maintains at 642.2 mAh g^{-1} after 20 cycles at the current density of 50 mA g^{-1}. The excellent electrochemical performance suggests that the electrode is a promising candidate for the next generation lithium ion batteries (LIBs).

Recently, tin-based oxides have been considered as the most promising anode materials in lithium-ion batteries [1-5]. Take SnO_2 for example, it exhibits a reversible capacity of 782 mAh g^{-1} with a theoretical capacity of 1494 mAh g^{-1} [4]. However, the cracking of tin-based oxide nanocrystals caused by a large volume change and the aggregation of metal components during charge and discharge process leads to capacity fading on cycling [6, 7], which limits their practical application. To overcome these problems, nano-sized SnO_2 materials with loose structures, such as nanotubes [8], nanowires [9], nanosheets [10], mesoporous and hollow structures [11, 12] were widely applied. Besides, some nonmetal oxides, metal oxides, and graphite were added to improve the electrochemical properties [13, 16]. And to date, a series of tin-based ternary oxides, such as M_2SnO_4 (M = Zn, Ba, Co, Mg) have been used as anode materials for lithium-ion batteries [4, 17-19] and exhibited a high charge-discharge capacity.

As an important member of tin-based oxide materials with a band gap of 3.6 eV, Zn_2SnO_4 has attracted considerable attention in recent years owing to its high electron mobility (10^{-15} cm^2 V^{-1} s^{-1}), high electrical conductivity (10^2~10^3 S cm^{-1}) and low visible absorption [20]. These outstanding properties enable it suitable for a wide range of applications such as anodes material in LIBs [4-7], photoelectrochemical cells [21], photocatalytic materials [22], dye-sensitized solar cells [20] and sensors for gas [23]. Recently, several groups have synthesized Zn_2SnO_4 nanostructures by various routes, including high temperature calcination [24], thermal evaporation [25], sol-gel method [26] and hydrothermal method [4, 5, 20]. In these methods, the hydrothermal synthesis technique has been widely used owing to its operational simplicity, cost-efficiency and the capability for large-scale production [27]. In recent years, more and more researchers have paid attention to the special morphology, such as octahedron, cube, globular and rod structures and so on, which have been synthesized by the hydrothermal method [28-32].

Herein, a hierarchical Zn_2SnO_4 octahedron decorated with nanoplates was fabricated via a facile surfactant-free hydrothermal method. When it is investigated as an anode material for LIBs, a high initial discharge capacity of 1629.9 mAh g^{-1} is obtained and the capacity maintains at 642.2 mAh g^{-1} after 20 cycles at the current density of 50 mA g^{-1}. The excellent electrochemical performance owing to the unique hierarchical architecture suggests that the electrode is a promising candidate for the next generation LIBs.

The surfactant-free and gram-scale synthesis of Zn_2SnO_4 octahedron decorated with nanoplates has been realized under hydrothermal conditions at 200 °C for 22 h. The detailed experiment process is described in the portion of experimental. The X-ray diffraction (XRD) pattern of as-prepared sample is shown in Fig. 1. It exhibits high crystallinity and a typical cubic structure, which is in accordance with those established by JCPDS card No. 24-1470 (space group: Fd-3m no. 227). No peaks of other impurity phases are detected from the pattern, indicating the high purity of the product.

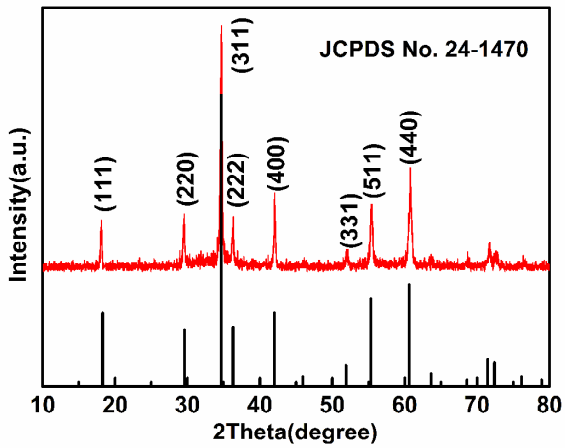

Fig. 1 The XRD pattern of as-prepared Zn_2SnO_4.

The measurements of the scanning electron microscopy (SEM) and the transmission electron microscopy (TEM) are examined to analyse the microstructure of as-prepared Zn_2SnO_4 in detail. The low magnification SEM image which is shown in Fig. 2a exhibits a uniform distribution of Zn_2SnO_4 octahedron decorated with nanoplates. According to the high magnification image (Fig. 2b),

RSC Advances Accepted Manuscript

the nanoplates grow along the edge of octahedron and some vertically distribute on each plane of the octahedron. The size of octahedron is about 2 μm, while the length of nanoplates is in the range of 200~400 nm and the thickness is about 20 nm.

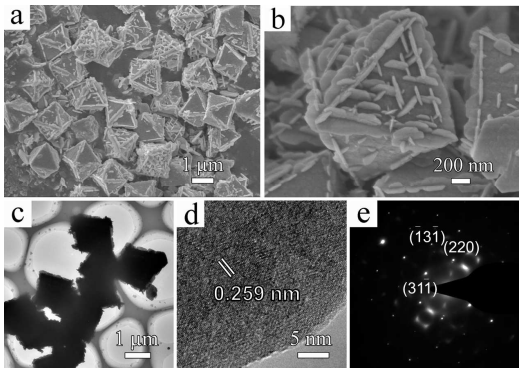

Fig. 2 (a, b) Typical low and high magnification SEM images, (c, d) TEM and HRTEM images and (e) SAED pattern of as-prepared Zn_2SnO_4.

Fig. 2c shows the low magnification TEM image, and it clearly confirms the observation in SEM images. In order to further investigate the structure of this microstructure, HRTEM and SAED are conducted on a scattering nanoplates, as shown in Fig. 2d, e. The lattice interplanar spacing is measured to be 0.259 nm, corresponding to the (311) plane of Zn_2SnO_4. Meanwhile, the SAED pattern indicates that the obtained Zn_2SnO_4 is single crystal structure.

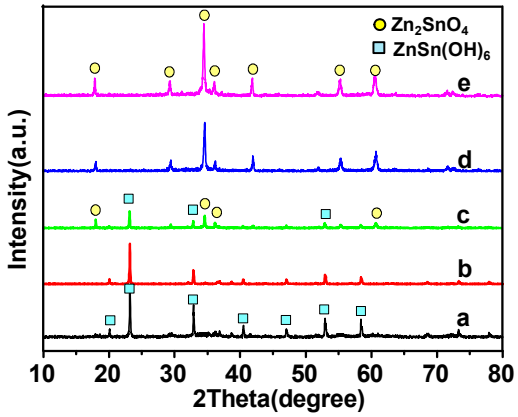

Fig. 3 XRD patterns of as-obtained products at different duration time: (a) 1 h, (b) 2 h, (c) 6 h, (d) 12 h and (e) 24 h.

To understand the formation process of unique Zn_2SnO_4 hierarchical structures and the possible growth mechanism, the time-dependent phase composition and morphological evolution process were examined by XRD and SEM. Fig. 3 shows the XRD patterns of as-obtained samples at different reaction time. When the reaction time reaches 1 h, only $ZnSn(OH)_6$ phase can be observed in the XRD pattern. Comparing with the product obtained at 1 h, the peaks of $ZnSn(OH)_6$ obtained after 2 h diminished gradually, and some weak diffraction peaks of Zn_2SnO_4 appear when the reaction time increases to 6 h. It is obvious that the intensity of Zn_2SnO_4 peaks increase with the increasing of duration time. When the reaction time is further increased to 12 h, all the diffraction peaks are assigned to Zn_2SnO_4 phase, indicating that the products completely evolve from $ZnSn(OH)_6$ to Zn_2SnO_4.

Fig. 4 shows the SEM images of different reaction durations, respectively. When the reaction time reaches 0.5 h, it can be observed that the sample is consisted by nanoparticles with a few tens of nanometers in diameter (Fig. 4a). As the process is prolonged to 1 h, nanoparticles are still the exclusive products, however, a small quantity of smooth-faced $ZnSn(OH)_6$ cubes emerge which can be seen in Fig. 4b. After 2 h, the products were almost uniform and regular cubes with an edge length about 1 μm.

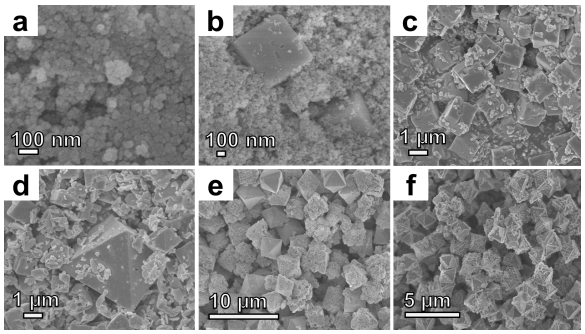

Fig. 4 SEM images of as-obtained products at different duration time: (a) 0.5 h, (b) 1 h, (c) 2 h, (d) 6 h, (e) 12 h and (f) 24 h

Meanwhile, some protuberances and erosions on the surface of the Zn_2SnO_4 cubes could be observed. With the reaction time up to 6 h, it can be seen that some Zn_2SnO_4 octahedrons with smooth surfaces appear among the cubes (Fig. 4d). At 12 h, all cubic $ZnSn(OH)_6$ turns into octahedral Zn_2SnO_4. In addition, a significant change could be observed in the morphology of the Zn_2SnO_4 microstructures. A part of octahedrons are decorated with nanoplates on their planes (Fig. 4e). When the reaction time was increased to 22 h, a uniform distribution of Zn_2SnO_4 octahedrons decorated with nanoplates was formed (Fig. 2a). No significant changes in the Zn_2SnO_4 octahedrons were observed even though the reaction time was further increased to 24 h (Fig. 4f).

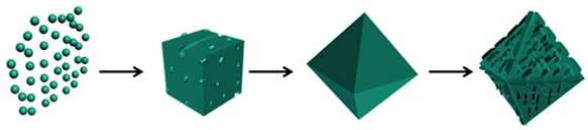

Fig. 5 Schematic illustration of the formation processes of Zn_2SnO_4 nanostructures.

On the basis of the experimental results, it is believed that the formation of Zn_2SnO_4 hierarchical structures is corresponding to the "crystallization–dissolution–recrystallization" growth mechanism [22, 28, 33-35]. The formation process of the Zn_2SnO_4 hierarchical structures is schematically illustrated in Fig. 5. In the first step, plenty of Zn^{2+}, Sn^{4+} and OH^- in the solution lead to massive precipitation of $ZnSn(OH)_6$ nuclei. Large amounts of cube-shaped $ZnSn(OH)_6$ crystals are further obtained with the continuous supply of the building blocks to the nuclei, which is structurally and energetically favourable [35]. With the increasing temperature and pressure steadily, the solubility of many oxides increases in water [22]. Thereby, $ZnSn(OH)_6$ gradually dissolve, leading to the protuberances and erosions present on the surface of the $ZnSn(OH)_6$ cubes. Subsequently, owing to the large solubility and metastability of $ZnSn(OH)_6$ compared with

RSC Advances Accepted Manuscript

This journal is © The Royal Society of Chemistry [year]

Zn_2SnO_4, this metastable intermediate phase decomposed and recrystallized to form Zn_2SnO_4 nuclei according to the "dissolution-recrystallization" mechanism [34]. The formation of the octahedral Zn_2SnO_4 microcrystal is believed to originate from a higher nuclei growth rate of {100} than {111} [28]. It is worth noting that Zn_2SnO_4 molecules generated rate at this stage slows down due to the low concentration of reactants. As a consequence, the concentration of Zn_2SnO_4 molecules is not enough for the former octahedron to grow from the circumference. The new generated building molecule blocks will preferentially occur at the active sites of the circumferential edges and planes which have relatively higher free energies than other sites on the surface [36]. Then, Zn_2SnO_4 nanoplates gradually generate on the active site of the octahedron and sparsely distribute on the basal planes to form the "texture-like" architectures, which are attributed to crystal lattice match between the growing facets of the nanoplates and the basal planes of the octahedron [28].

Zn_2SnO_4 is regarded as a very appealing candidate for anode material for LIBs and adopted as highly electrical conductive cores for supercapacitors electrodes recently. In the present work, the as-prepared Zn_2SnO_4 is evaluated as anode electrode for LIBs. Fig. 6a shows the Cyclic Voltammetry (CV) curves of the Zn_2SnO_4 electrode at a scan rate of 0.2 mV s^{-1} with potential windows ranging from 0.01 to 3 V. For the first discharge process, two cathodic peaks are located at 0.1 V and 0.55 V, corresponding to the multi-step electrochemical lithium reaction process (Equ. 1a, 1b). There is a main cathodic peak at 0.65 V and a shoulder at 1.0 V observed during the subsequent cycles. During the charge process, anodic peaks at 0.6 V and 1.45 V are observed ranging from the first to the third cycle. The good overlap ratio of the second and third cycle indicates a fascinating cycling performance of the electrode. The formation and deformation of Li_2O is able to occur when the voltage is higher than 1 V. The reversible reactions of Equ. 1a and 1b take place to some extent when the pair redox peaks exhibit at 0.1/0.45 V. Meanwhile, the redox peaks at 0.55/0.65 V is related to the alloying/dealloying processes of Li_xZn and Li_xSn, shown as Equ. 2 and 3. Accroding to the above discussion, the charge/discharge processs can be described as follows:

$$4Li^+ + Zn_2SnO_4 + 4e^- \rightarrow Sn + 2Li_2O + 2ZnO \quad (1a)$$

$$8Li^+ + Zn_2SnO_4 + 8e^- \rightarrow 2Zn + Sn + 4Li_2O \quad (1b)$$

$$x\,Li^+ + Sn + x\,e^- \leftrightarrow Li_xSn, x \le 4.4 \quad (2)$$

$$y\,Li^+ + Zn + y\,e^- \leftrightarrow Li_yZn, y \le 1 \quad (3)$$

Fig. 6b shows the first three charge and discharge curves of the LIBs applying Zn_2SnO_4 as anode electrode at the current density of 50 mA g^{-1}. The Zn_2SnO_4 electrode shows an initial discharge and charge capacity of 1629.9 mAh g^{-1} and 928.7 mAh g^{-1}, respectively. Meanwhile, the discharge plateaus at ~0.65 V, ~0.15 V and charge plateaus at ~0.6 V, ~1.0 V are corresponding to the results of CV. Owing to the formation of the solid electrolyte interface (SEI) film and the decomposition of electrolyte, the initial coulombic efficiency is only 56.98%. However, there is a small capacity loss between the second and third discharge capacities, which further suggests an excellent electrochemical performance of the electrode.

Cycling performance is also an important standard to evaluate the electrochemical performance of electrodes. As Fig. 6c shown, the Zn_2SnO_4 electrode shows an excellent performance at the current density of 50 mA g^{-1}. Comparing with the second discharge capacity, the discharge capacity maintained at 642.2 mAh g^{-1} after 20 cycles with the capacity retention ratio of 62.91%. Even at the rate of 100 mA g^{-1}, the specific discharge capacities at the end of 20 cycles remains as high as 543.5 mAh g^{-1}.

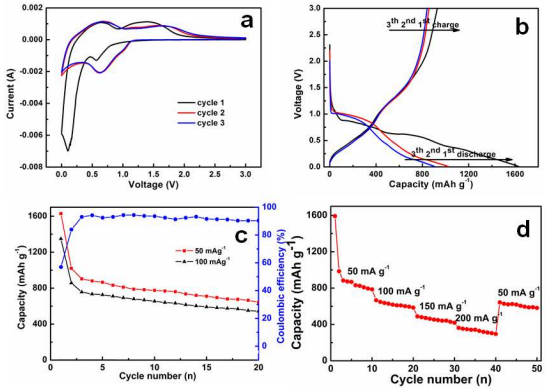

Fig. 6 (a) Initial three CV curves at the scan rate of 0.2 mV s^{-1}, (b) typical charge/discharge curves, (c) cycling performance and coulombic efficiency at the current density of 50 mA g^{-1} and 100 mA g^{-1}, (d) rate capability at various current densities.

The rate capability of the battery is shown in Fig. 6d. The battery shows a better rate capability obviously, when the rate is increased stepwise from 50 mA g^{-1} to 200 mAh g^{-1}, a stable capacity of about 305.9 mAh g^{-1}can be achieved. Remarkably, when the current density is again reduced back to 50 mA g^{-1}, a stable high capacity of 581.5 mAh g^{-1} can be resumed. The excellent electrochemical performance of the Zn_2SnO_4 is mainly contributed to both small grain size and more active sites provided by the "texture-like" architectures [35, 37].

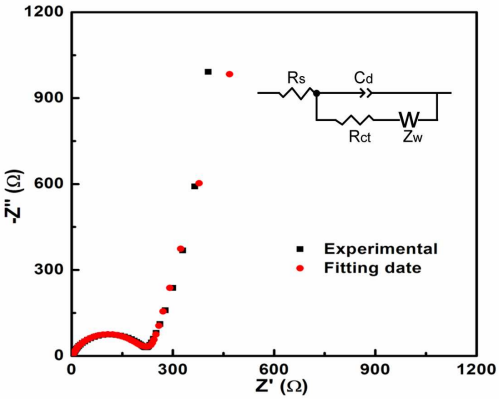

Fig. 7 Nyquist plots of as-prepared Zn_2SnO_4 measured at open circuit potential and the corresponding equivalent circuit (inset).

Electrochemical impedance spectroscopy (EIS) is usually measured to investigate the electrochemical resistances, such as electrolyte/electrode interface, charge transfer and lithium-ion diffusion resistances. Fig. 7 shows the Nyquist plot of as-prepared Zn_2SnO_4 measured at open circuit potential and the corresponding equivalent circuit is shown as inset. The semicircle

RSC Advances Accepted Manuscript

in high frequency of the curve stands for the charge-transfer resistance and the inclined line is related to the diffusion resistance of lithium-ion. After fitting the experimental data, the charge-transfer and Warburg resistances are as low as 221.72 and 5.65 Ω, respectively, indicating fast electrochemical reaction and lithium diffusion processes. It also suggests Zn_2SnO_4 is an ideal candidate for LIBs.

In summary, Zn_2SnO_4 octahedron decorated with nanoplates has been successfully prepared via a facile surfactant-free hydrothermal method. As an anode material for LIBs, Zn_2SnO_4 octahedron exhibits excellent electrochemical performance, suggesting a potential application in the second rechargeable LIBs.

Experimental

Synthesis of Zn_2SnO_4 octahedron decorated with nanoplates

All the chemicals were analytical grade and used without further purification. The detailed process for the synthesis was as follows: $SnCl_4 \cdot 5H_2O$, $Zn(CH_3COO)_2 \cdot 2H_2O$ and NaOH were mixed with molar ratio of 2:1:8. The mixture was kept on stirring for 15 minutes and then transferred into a teflon lined steel autoclave with a capacity of 30 mL, maintained at 200 ^oC for 22 h. After complete reaction, the autoclave cooled to room temperature naturally. Precipitates were centrifuged, sequentially washed with water and ethanol for several times to remove the ions possibly remaining in the products, and finally dried at 80 ^oC for 12 h in a vacuum.

Characterization:

The crystalline structures of the as-prepared samples were characterized by XRD spectra (Rigaku D/Max-2500, Cu Kα radiation, λ=0.1518 nm). The morphologies were detected by SEM on a JEOL JSM-6700F (Field Emission) scanning electron microscope, TEM and HRTEM on a Tecnai G2 F20 TEM.

Electrochemical measurements:

The as-prepared Zn_2SnO_4 octahedron decorated with nanoplates was used as the anode material for LIBs. For the preparation of the electrodes, the active material, acetylene black and binder (PVDF) in a weight ratio of 80:10:10 were mixed in N-methyl-2-pyrrolidone (NMP). The resultant slurry, pasted on Cu foil, was dried at 100 °C under vacuum for 10 h. Then the cells were assembled in an argon-filled glove box using lithium metal as the counter electrode, and 1 M $LiPF_6$ (dissolved in ethylene carbonate (EC), ethylene methyl carbonate (EMC) and dimethyl carbonate (DMC) with a 1:1:1 volume ratio) as the electrolyte. Cells were tested at room temperature using LAND-CT2001A battery cycler (Wuhan, China) within the voltage range of 0.01-3 V (vs. Li^+/Li). CV and EIS were performed on a CHI660B electrochemical workstation.

This work was supported by the National Natural of Science Foundation of China (Grant No. 21371101), 111 Project (B12015) and MOE Innovation Team (IRT13022) of China.

Notes and references

[a]*Department of Materials Chemistry, Key Laboratory of Advanced Energy Materials Chemistry (MOE), TKL of Metal and Molecule-based Material Chemistry, College of Chemistry Nankai University, Tianjin, 300071, P. R. China.*
[b]*Collaborative Innovation Center of Chemical Science and Engineering (Tianjin), Tianjin 300072, P. R. China.*
E-mail: zhwj@nankai.edu.cn

1 M. Tsaroucha, Y. Aksu and E. Irran, *Chem. Mat.,* 2011, **23**, 2428-2438.
2 Z. Wang, D. Luan and F. Y. C. Boey, *J. Am. Chem. Soc.,* 2011, **133**, 4738-4741.
3 J. Li, Y. Zhao and N. Wang, *Chem. Commun.*, 2011, **47**, 5238-5240.
4 A. Rong, X. P. Gao and G. R. Li, *J. Phys. Chem. B*, 2006, **110**, 14754-14760.
5 X. J. Zhu, L. M. Geng and F. Q. Zhang, *J. Power Sources,* 2009, **189**, 828-831.
6 K. Kim, A. Annamalai and S. H. Park, *Electrochim. Acta,* 2012, **76**, 192-200.
7 X. Zheng, Y. Li and Y. Xu, *CrystEngComm*, 2012, **14**, 2112-2116.
8 Y. Wang, J. Y. Lee and H. C. Zeng, *Chem. Mat.,* 2005, **17**, 3899-3903.
9 Y. Han, X. Wu and Y. Ma, *CrystEngComm,* 2011, **13**, 3506-3510.
10 C. Wang, Y. Zhou and M. Ge, *J. Am. Chem. Soc.,* 2009, **132**, 46-47.
11 R. Demir-Cakan, Y. S. Hu and M Antonietti, *Chem. Mat.,* 2008, **20**, 1227-1229.
12 X. W. Lou, Y. Wang and C. Yuan, *Adv. Mater.,* 2006, **18**, 2325-2329.
13 L.Yuan, K. Konstantinov and G. X. Wang. *J. Power Sources,* 2005, **146**, 180-184.
14 X. W. Lou, J. S. Chen and P. Chen, *Chem. Mat.,* 2009, **21**, 2868-2874.
15 X. W. Lou, C. M. Li and L. A. Archer. *Adv. Mater.,* 2009, **21**, 2536-2539.
16 S. Ding, D. Luan and F. Y. C. Boey, *Chem. Commun.*, 2011, **47**, 7155-7157.
17 S. S. Shin, J. S. Kim and J. H. Suk, *ACS nano,* 2013, **7**, 1027-1035.
18 J. Zhang, J. Liang and Y. Zhu, *J. Mater. Chem. A*, 2014, **2**, 2728-2734.
19 K. N. Kim, H. K. Jung and H. D. Park, *J. Lumin.,* 2002, **99**, 169-173.
20 B. Tan, E. Toman and Y. Li, *J. Am. Chem. Soc.,* 2007, **129**, 4162-4163.
21 M. A. Alpuche-Aviles, Y. Wu, *J. Am. Chem. Soc.,* 2009, **131**, 3216-3224.
22 J. Zeng, M. D. Xin and K. W. Li, *J. Phys. Chem. C*, 2008, **112**, 4159-4167.
23 Z. Chen, M. Cao and C. Hu, *J. Phys. Chem. C*, 2011, **115**, 5522-5529.
24 Y. Du, P. Ding, *J. Alloy. Compd.,* 2010, **502**, L14-L16.
25 L. Wang, X. Zhang and X. Liao, *Nanotech.*, 2005, **16**, 2928.
26 G. Fu, H. Chen and Z. Chen, *Sens. Actuators B: Chem.,* 2002, **81**: 308-312.
27 H. Zhu, D. Yang and G. Yu, *J. Phys. Chem. B*, 2006, **110**, 7631-7634.
28 Z. Li, Y. Zhou and J. Zhang, *Cryst. Growth Des.,* 2012, **12**, 1476-1481.
29 J. Wang, X. W. Sun and S. Xie, *Cryst. Growth Des.,* 2007, **8**, 707-710.
30 M. Miyauchi, Z. Liu and Z. G. Zhao, *Chem. Commun.,* 2010, **46**, 1529-1531.
31 Z. Li, Y. Zhou and C. Bao, *Nanoscale,* 2012, **4**, 3490-3494.
32 Y. F. Wang, K. N. Li and Y. F. Xu, *Nanoscale,* 2013, **5**, 5940-5948.
33 Y. Q. Jiang, C. X. He and R. Sun, *Mater. Chem. Phys.,* 2012, **136**, 698-704.
34 X. Ji, X. Huang and J. Liu, *J. Alloy. Compd.,* 2010, **503**, L21-L25.
35 Y. Zeng, T. Zhang and H. Fan, *J. Phys. Chem. C*, 2009, **113**, 19000-19004.
36 X. M. Ni, Q. B. Zhao and H. G. Zheng, *Eur. J. Inorg. Chem.* 2005, 4788-4793.
37 L. Di, Q. Qin and W.Z. Zheng, *ACS Appl. Mater. Interfaces*. 2013, **5**, 9095-9100.

RSC Advances Accepted Manuscript

This journal is © The Royal Society of Chemistry [year]